The Geological Society of America
Special Paper 465
2010

Elliptical craters and basins on the terrestrial planets

Jeffrey C. Andrews-Hanna
Department of Geophysics and Center for Space Resources, Colorado School of Mines, Golden, Colorado 80401, USA

Maria T. Zuber
Department of Earth, Atmospheric, and Planetary Sciences, Massachusetts Institute of Technology, Cambridge, Massachusetts 02139, USA

ABSTRACT

The four largest well-preserved impact basins in the solar system, Borealis, Hellas, and Utopia on Mars, and South Pole–Aitken on the Moon, are all significantly elongated, with aspect ratios >1.2. This population stands in contrast to experimental studies of impact cratering that predict <1% of craters should be elliptical, and the observation that ~5% of the small crater population on the terrestrial planets is elliptical. Here, we develop a simple geometric model to represent elliptical crater formation and apply it to understanding the observed population of elliptical craters and basins. A projectile impacting the surface at an oblique angle leaves an elongated impact footprint. We assume that the crater expands equally in all directions from the scaled footprint until it reaches the mean diameter predicted by scaling relationships, allowing an estimate of the aspect ratio of the final crater. For projectiles that are large relative to the size of the target planet, the curvature of the planetary surface increases the elongation of the projectile footprint for even moderate impact angles, thus increasing the likelihood of elliptical basin formation. The results suggest that Hellas, Utopia, and South Pole–Aitken were formed by impacts inclined at angles less than ~45° from horizontal, with a probability of occurrence of ~0.5. For the Borealis Basin on Mars, the projectile would likely have been decapitated, with the topmost portion of the projectile on a trajectory that did not intersect with the surface of the planet.

INTRODUCTION

While the vast majority of impact craters are roughly circular in planform, a small fraction of craters produced both experimentally and observed on planetary surfaces have significantly elongated shapes. Experimental work suggests that these elliptical craters form in only the most oblique impacts, and the critical impact angle for elliptical crater formation (θ_c, representing the angle between the projectile trajectory and the horizontal) is 4.7° (Gault and Wedekind, 1978). For a population of projectiles with random trajectories, the probability of an impact occurring at an angle of less than a given angle, θ, is $\sin^2(\theta)$ (Gilbert, 1893), irrespective of the gravity of the target planet (Shoemaker, 1962). Thus, the experimentally determined threshold angle for elliptical crater formation would suggest that ~0.7% of craters should be elliptical.

However, surveys of the observed population of elliptical craters on Mars, Venus, and the Moon found that roughly 5% of

Andrews-Hanna, J.C., and Zuber, M.T., 2010, Elliptical craters and basins on the terrestrial planets, *in* Gibson, R.L., and Reimold, W.U., eds., Large Meteorite Impacts and Planetary Evolution IV: Geological Society of America Special Paper 465, p. 1–13, doi: 10.1130/2010.2465(01).

the population of small (<150 km diameter) craters are elliptical (Schultz and Lutz-Garihan, 1982; Barlow, 1988; Bottke et al., 2000). Schultz and Lutz-Garihan (1982) proposed that for Mars, this paradox could be resolved if the planet possessed a population of small moons that spiraled inward to strike the surface at low angles. However, using a simple conceptual model of elliptical crater formation to reconcile the frequency of elliptical craters produced experimentally with that observed on the terrestrial planets, Bottke et al. (2000) found that such a scenario is not necessary. They assumed that the tendency of an impact to produce an elliptical crater is related to the ratio between the final crater diameter (D_c) and the projectile diameter (d_p). They considered results from two different experimental studies, investigating impacts into sand (Gault and Wedekind, 1978) and aluminum (Christiansen et al., 1993), with different D_c/d_p ratios and θ_c values. Bottke et al. (2000) used the results from these two studies to generalize an empirical power-law relationship between θ_c and D_c/d_p:

$$\theta_c = \theta_0(D_c/d_p)^m, \quad (1)$$

where $\theta_0 = 68.1°$, and m = –0.648. Utilizing the D_c/d_p ratio indicated by π-scaling relationships (Holsapple and Schmidt, 1982; Melosh, 1989), this power law successfully explains the 5% abundance of impact craters on the terrestrial planets, and it suggests that θ_c will also depend on projectile diameter.

At the other end of the size spectrum, the small population of the largest impact basins reveals a further discrepancy between the expected and observed population of elliptical impact craters. Here, we show that four of the six largest well-preserved impact basins in the solar system (Borealis, Hellas, and Utopia on Mars, and South Pole–Aitken on the Moon) all exhibit pronounced elliptical shapes. Of the basins we classify as "giant impact basins," which are defined as a basin diameter greater than half the planetary radius, only Caloris on Mercury and Imbrium on the Moon fall short of our assumed criterion for classification as an elliptical basin. Adopting the 5% abundance of elliptical craters observed in the small crater population, the probability that four of the six giant basins would be elliptical by random chance is 8.5×10^{-5}, and thus can be effectively ruled out.

We suggest that this paradox can be resolved by considering the effect of the curvature of the planetary surface on the resulting basin shape. For the largest impacts, the surface of the planet curves away from the projectile path, leading to more elongated projectile footprints (the projection of the projectile onto the surface of the planet). This increased elongation of the projectile footprint for a given impact angle increases the probability of elliptical basin formation. We developed a simple geometrical model for elliptical crater formation based on the calculated projectile footprint aspect ratio and the final crater diameter from π-scaling relationships. The model can explain both the critical angle in small-scale laboratory experiments and the observed fraction of elliptical craters in the 1–150-km-diameter range, and it further offers the expectation that a Hellas-sized impact basin would have a probability of being elliptical of ~0.4.

OBSERVED ELLIPTICAL BASINS ON MARS AND THE MOON

Known Impact Basins

While several studies have considered the statistics of small crater shapes (Schultz and Lutz-Garihan, 1982; Bottke et al., 2000), there has been less attention paid to the shapes of the giant impact basins. Since we are interested in the effect of the curvature of the surface on the resulting basin shape, we impose an arbitrary cutoff on what is considered a "giant" impact basin, considering here those basins having diameters >50% of the planetary radius.

In order to compare the observed basin dimensions with the predictions of scaling models, we focus on the diameter of the primary topographic rim of the basin (D_c), which we equate with the postmodification excavation cavity. Since the nonmascon basins are largely isostatic today, the topographic rim should also correspond with the basin rim in the lower-resolution crustal thickness data that was used as a proxy for the excavation cavity by Wieczorek and Phillips (1999). We describe this as the primary topographic basin, since the observed topography and crustal thickness will reflect the postimpact modification of the transient excavation cavity. The exterior and interior rings associated with many basins are generally characterized by a weaker expression in both topography and crustal thickness models, and are likely a product of the multiring basin modification process (Wieczorek and Phillips, 1999).

The primary topographic basin rim is traced just above the steep slope leading down into the main basin cavity, making use of both color topography (Fig. 1) and contour maps (not shown). The best-fit ellipse matching the basin rim is calculated by iterating the ellipse orientation, and major and minor axes in order to minimize the root mean square (RMS) misfit. Basin dimensions are here reported to 10 km precision, though it should be recognized that the uncertainty in identifying the main topographic rim exceeds this in some cases. These basin dimensions differ from previously reported measurements in some cases. However, for the purpose of this study, it is preferable to maintain a consistent methodology throughout, rather than to adopt the measurements of previous studies that have employed different criteria in basin rim identification.

The Hellas Basin on Mars is perhaps the best preserved of the giant impact basins, and it has been recognized as an elliptical structure produced by an oblique impact (Tanaka and Leonard, 1995). We reprojected the Mars Orbital Laswer Altimeter (MOLA) topography (Smith et al., 2001) of Hellas in a basin-centered polar coordinate system (Fig. 1A), preserving both the distance and angle between all points and the basin center. The dimensions of the primary topographic rim of the basin are found to be 2280 km by 1590 km (Table 1), and the ratio between the

major and minor axes (A/B) is 1.43. The ratio of the mean basin diameter to the planetary radius (D_c/r_p) is 0.57.

The shape of the Utopia Basin on Mars (McGill, 1989) is not as immediately apparent. While Utopia likely started out as an isostatically compensated basin with a depth comparable to that of Hellas, it was subsequently filled with volcanic, sedimentary, and eolian material, resulting in a pronounced positive gravity anomaly (Smith et al., 1999; Searls et al., 2006). Rather than examining the considerably muted topographic signature (Fig. 1B) or the distribution of tectonic features within and surrounding the basin, we focused on the crustal structure in order to estimate the original basin dimensions. We used a spherical harmonic membrane-flexural model (Banerdt, 1986; Banerdt and Golombek, 2000) to invert the gravity (Zuber, 2008) and topography (Smith et al., 2001) of Mars in order to isolate the isostatic crustal roots representing the prefill basin topography (Andrews-Hanna et al., 2008). In short, this method divides the crust into surface loads and isostatic roots that, together with the resulting membrane and flexural displacement, reproduce the observed gravity and topography. By applying this technique to Mars, and plotting the prefill topography in a Utopia-centered polar projection (Fig. 1C), we find the dimensions of the primary pre-fill topographic basin to be 2400 km by 2000 km (accounting for the lower resolution of the gravity data), corresponding to an aspect ratio of 1.2, and D_c/r_p of 0.65.

The observed basin size in the isostatic roots is substantially smaller than the 3200-km-diameter circular basin found by Thomson and Head (2001) and the 3380-km-diameter basin found by Frey (2008a). This discrepancy may be explained by noting the apparent ring structure that surrounds Utopia in the isostatic root map, leading to a surface expression in the topography and tectonic features that was interpreted as the basin rim

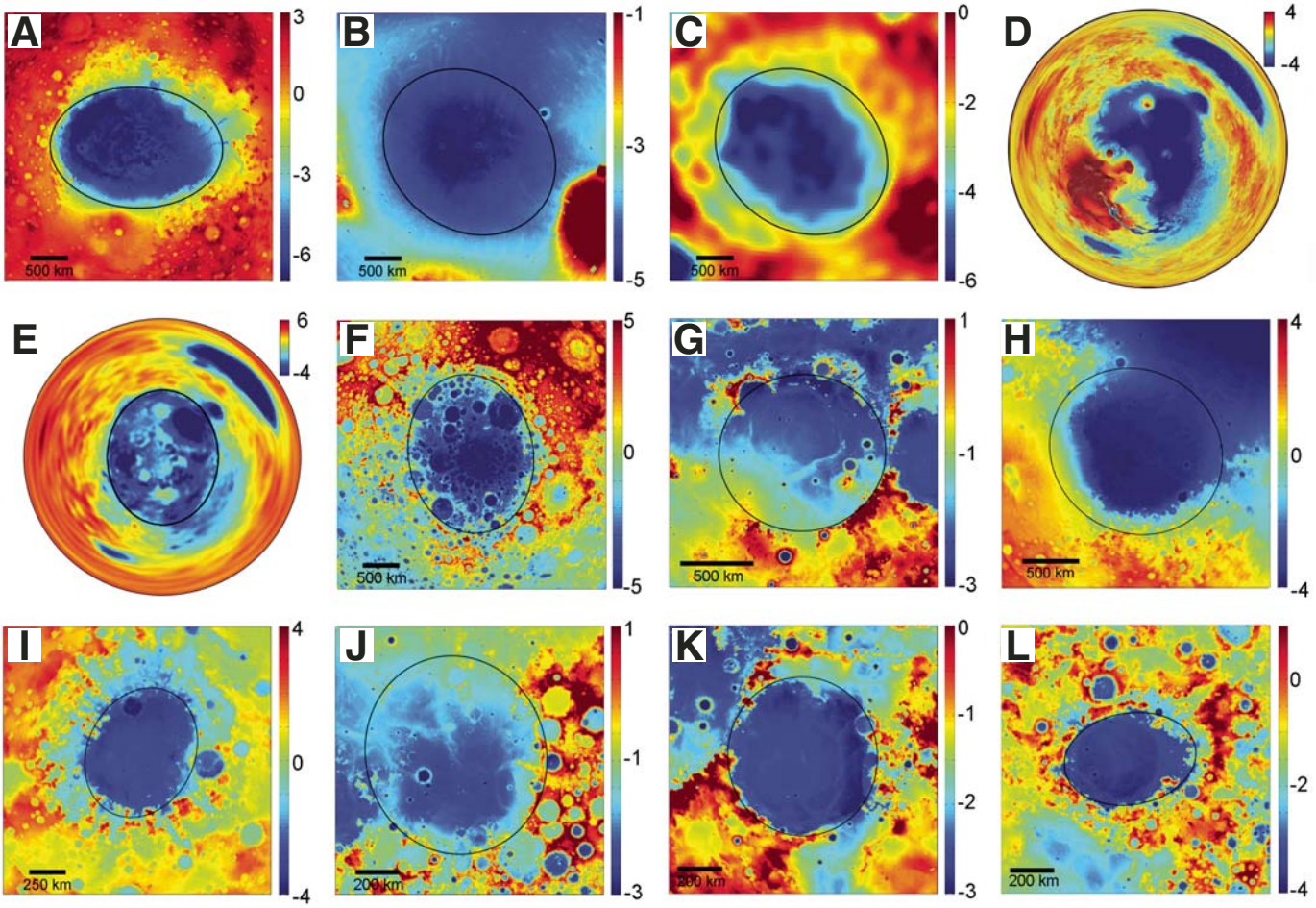

Figure 1. Basin-centered polar projection topographic maps of the largest known and proposed impact basins on Mars and the Moon (units on the color bars are km). The best-fit ellipses to the preserved rims are shown. The basins qualifying as giant impact basins ($D_c > 0.5\ R_p$) include Hellas (A), Utopia (B, in present-day topography; C, in modeled prefill topography), and Borealis (D, in present-day topography; E, in reconstructed pre-Tharsis topography) on Mars; and South Pole–Aitken (F) and Imbrium (G) on the Moon. Expanding the definition to include all basins greater than 500 km in diameter includes Isidis (H) and Argyre (I) on Mars; and Nubium (J), Serenitatis (K), and Crisium (L) on the Moon. Global polar projection maps (D–E) are circular, and introduce large distortions in features not centered on the origin (e.g., the Hellas Basin in D). Points along the rims for ellipse fitting were selected in regions that have escaped subsequent modification by impact, volcanic, and fluvial processes.

TABLE 1. OBSERVED BASIN DIMENSIONS AND MODEL PREDICTIONS

Basin	D_c* (km)	A† (km)	B§ (km)	A/B# (km)	$d_p \sin(\theta)^{1/3}$ ** (km)	θ_c†† (°)	d_p'§§ (km)	$P(\theta<\theta_c)$ ##	$d_p \sin(\theta)^{1/3}$ (W&S)*** (km)	θ_c (W&S)*** (°)	d_p' (W&S)*** (km)	$P(\theta<\theta_c)$ (W&S)***
Borealis	9550	10,600	8500	1.25	4369	(78)	4401	0.96	1480	(51)	1612	0.62
Utopia	2200	2400	2000	1.20	669	40	775	0.41	275	24	372	0.17
Hellas	1940	2280	1590	1.43	561	38	659	0.38	235	23	322	0.15
South Pole–Aitken	2060	2330	1780	1.31	481	44	550	0.48	215	32	266	0.28
Caloris†††	1550	1525	1315	<1.2	337	33.4	–	0.30	149	24	–	–
Imbrium	1120	1140	1090	<1.2	221	33	–	0.30	107	24	–	–
Isidis	1500	1570	1430	<1.2	405	34	–	0.31	175	21	–	–
Nubium	860	900	810	<1.2	156	30	–	0.25	79	22	–	–
Serenitatis	690	710	670	<1.2	119	27	–	0.21	61	20	–	–
Crisium	510	600	420	1.43	81	25	108	0.18	43	18	64	0.10

*Mean basin diameter.
†Basin semi-major axis.
§Basin semi-minor axis.
#Basin aspect ratio (if less than 1.2, the basin is not considered elliptical).
**Projectile diameter as a function of impact angle θ from the π-scaling relationship.
††Critical angle for elliptical crater formation from the π-scaling relationship. Value in parentheses gives critical angle for projectile decapitation if this occurs prior to onset of crater ellipticity.
§§Projectile diameter at the onset of basin ellipticity (if observed basin is elliptical).
##Probability of an impact occurring at or below the critical angle for basin ellipticity.
***As before, but for the energy-scaling relationship of Wilhelms and Squyres (1984) (W&S).
†††The Caloris Basin dimensions were taken from Fassett et al. (2009) and thus may not compare directly with measurements made in this study.

in those studies. The relief in the isostatic roots across the basin rim identified here is a factor of 3–5 times greater than that across the outer ring structure. Even in well-preserved lunar basins, discrimination between the primary basin cavity and surrounding ring structures requires careful consideration of the topography and/or crustal thickness (Wieczorek and Phillips, 1999). For the case of Utopia, the topographic signature is highly muted, and the crustal thickness models also include the voluminous fill within and surrounding the basin (Searls et al., 2006). The gravity-topography inversion utilized here distinguishes between the prefill isostatically compensated basin and the later flexurally supported fill, thereby providing a more accurate characterization of the original basin. We find similar basin dimensions utilizing crustal thickness models (Neumann et al., 2008), though the relief across the primary basin rim is diminished relative to that across the outer ring.

The Borealis Basin on Mars, encompassing the northern lowlands, is the largest proposed impact structure in the solar system. Wilhelms and Squyres (1984) first suggested that the northern lowlands of Mars may be the expression of a single giant impact basin. Subsequent studies often dismissed the possibility of an impact origin for the Martian crustal dichotomy, primarily due to the fact that the present-day lowlands cannot be fit with a single circular impact basin (McGill and Squyres, 1991), since the proposed circular basin leaves ~40% of the lowlands unaccounted for. However, Andrews-Hanna et al. (2008) used an inversion of the gravity and topography to trace the dichotomy boundary beneath Tharsis and found that the resulting globally continuous dichotomy boundary is accurately fit by an ellipse measuring 10,600 km by 8500 km. This elliptical basin is characterized by a ratio between the major and minor axes (A/B) of 1.25, and a ratio of the mean basin diameter to the planetary radius (D_c/r_p) of 2.81. Projections of the Borealis Basin in a basin-centered polar coordinate system (Figs. 1D and 1E) bear a striking resemblance to the much smaller Hellas, Utopia, and South Pole–Aitken Basins (Figs. 1A, 1C, and 1F), though it is a factor of four greater in size. The elliptical shape and bimodal crustal thickness distribution of this Borealis Basin strongly support an origin through an oblique impact. An impact origin for the dichotomy is further supported by simulations demonstrating the feasibility of such a giant impact (Marinova et al., 2008; Nimmo et al., 2008), and the tentative interpretation of Arabia Terra as a partial multiring structure around the basin (Andrews-Hanna et al., 2008).

The largest recognized impact basin on Earth's Moon is the South Pole–Aitken Basin, which also exhibits an elliptical shape (Garrick-Bethell and Zuber, 2009) in both topography and elemental abundance data (Smith et al., 1997; Lawrence et al., 2002; Lawrence et al., 2003). Plotting the topography (Smith et al., 2009a, 2009b; Zuber et al., 2009) in a basin-centered polar coordinate system (Fig. 1F), we find the primary topographic basin dimensions to be 2330 km by 1780 km, corresponding to an aspect ratio of 1.31 and D_c/r_p of 1.18. This basin aspect ratio is similar to the main topographic rim found by Garrick-Bethell and Zuber (2009), though the basin dimensions are slightly larger due to the application of different criteria in identifying the rim. While slightly smaller than Hellas and Utopia in absolute size, South Pole–Aitken is substantially larger relative to the planetary radius. The Imbrium Basin on the Moon also falls into the category of a giant impact basin. The primary basin diameter in crustal thickness models has been estimated as 895 km (Hikida and Wieczorek, 2007). In order to maintain a consistent methodology, we reanalyzed the basin in Lunar Orbiter Laser Altimeter (LOLA) topography (Smith et al., 2009a, 2009b; Zuber et al., 2009) and found the diameter of the main topographic rim to be

1120 km (D_c/r_p = 0.64; Fig. 1G), consistent with the results of Spudis (1993). This discrepancy is a result of the use of different conventions and data sets in identifying the rim. The basin is nearly circular, with A/B = 1.05.

On Mercury, only the Caloris Basin, with an estimated diameter of 1550 km (D_c/r_p = 0.64), fits the adopted criterion of a giant basin (Murchie et al., 2008). The first full-basin images obtained by *MESSENGER* revealed an approximately circular basin (Murchie et al., 2008). Recent mapping of the basin-related units and sculpture has suggested a slightly elliptical basin with dimensions of 1525 km by 1315 km and an aspect ratio of 1.16 (Fassett et al., 2009), though this still falls short of our minimum criterion for consideration as an elliptical basin. While Caloris and Imbrium are the smallest of the giant basins considered here, their sizes relative to the planetary radius (D_c/r_p ~0.6) are similar to Hellas and Utopia on Mars. Of the six basins we classify as giant impact basins, only Caloris and Imbrium fall short of the criterion we adopt for elliptical basins of an aspect ratio of 1.2. However, even these two basins exhibit significant departures from circularity. At the scale of the largest impact basins, a circular outline appears to be the exception rather than the rule.

A decrease in the requirement for consideration as a "giant" impact basin to a simple diameter cutoff of 500 km would include the Isidis (D_c = 1500 km; A/B < 1.2) and Argyre (780 km; A/B = 870 km/690 km = 1.26) Basins on Mars (Figs. 1H and 1I). Several additional basins with diameters greater than 500 km have been identified on Mars (Barlow crater database, available online at http://webgis.wr.usgs.gov/). However, we find that the primary topographic basins exhibit diameters less than 500 km in MOLA topography, or have experienced significant erosion and relaxation (Mohit and Phillips, 2007), which prevent an accurate determination of the basin size and shape. Nevertheless, these basins are all approximately circular in outline. Many possible buried impact basins in various states of degradation have been identified on Mars using MOLA topography and crustal thickness models (Frey et al., 2002; Frey, 2006, 2008a), but we do not include these in the present discussion due to the difficulties in identifying the primary topographic basin rim and shape of these poorly expressed basins. These "quasi-circular depressions" are characterized by extremely shallow depth and/or weak expression in crustal thickness models, suggesting that they are either in an extreme state of relaxation or are substantially infilled. As a result, unambiguous identification of the primary basin rim, as opposed to a larger outer ring structure, is not possible. Furthermore, inclusion of quasi-circularity in the criteria for basin identification might bias the results toward circular rather than elliptical structures. We have limited this study to those basins with either a clear and well-preserved topographic expression or, in the case of Utopia, a clear gravitational expression that enables us to reconstruct the prefill topography.

Many confirmed and possible impact basins greater than 500 km in diameter have been identified on the Moon (Wilhelms, 1987; Frey, 2008b), though the partial preservation of many of the basins often makes determination of the basin size and shape difficult. We again limit ourselves to the well-preserved basins for which the primary topographic rim corresponding to the modified excavation cavity can be identified. We analyzed all "definite" lunar basins (Wilhelms, 1987) larger than 500 km in diameter using LOLA topography (Smith et al., 2009a, 2009b; Zuber et al,. 2009). We excluded basins for which the topographic signature was degraded such that the basin rim could not be clearly identified around the majority of the circumference (e.g., Fecunditatis, Tranquilitatis). For basins with a pronounced multiring structure, the innermost significant topographic ring was chosen as the main basin rim, as suggested for Orientale (Wieczorek and Phillips, 1999; Hikida and Wieczorek, 2007). Thus, some basins previously identified as being greater than 500 km in diameter were found to be substantially smaller, and were excluded (e.g., Hertzprung). We also found a slightly smaller diameter of ~450 km in the topography for the basin Smythii than that found in crustal thickness models (Hikida and Wieczorek, 2007). While the basin diameter from the crustal thickness model may be more accurate, we excluded this basin for the sake of consistency. The remaining basins greater than 500 km in diameter include the Nubium (D_c = 860 km, A/B = 900 km/810 km = 1.11), Serenitatis (D_c = 690 km, A/B = 710 km/670 km = 1.06), and Crisium (D_c = 510 km, A/B = 600 km/420 km = 1.43) Basins (Figs. 1J–1L). Of these, only Crisium is significantly elongated. There is significant uncertainty in these basin diameters and dimensions due to the difficulty in assigning the primary topographic rim. Venus possesses no confirmed basins that can be considered giant impact basins (Phillips et al., 1991).

Unconfirmed Possible Giant Impact Basins

While Borealis, Hellas, Utopia, South Pole–Aitken, Imbrium, and Caloris are the largest clearly expressed impact basins in the solar system, several other megabasins have been proposed. It has been suggested that a single impact basin can be circumscribed around the majority of the nearside maria, termed either the "Gargantuan" (Cadogan, 1974) or "Procellarum" (Whitaker, 1980) Basin. An impact origin for this region is highly uncertain, and the location of the rim of the proposed basin is poorly defined and cannot be fit by an ellipse with a reasonable degree of accuracy. Much of the basin "rim" can be ascribed to other impact features, no clear rim can be identified around much (~40%) of the basin, and there exist large areas of unexplained high topography within the putative basin.

A much larger basin has been suggested to explain the lunar crustal and topographic asymmetry, with the basin cavity explaining the thinner crust and lower topography of the lunar nearside (Byrne, 2007). However, unlike the Martian crustal dichotomy, the lunar crustal distribution is best described as an asymmetry and is accurately represented by a spherical harmonic degree-one variation in the crustal thickness. The resulting unimodal crustal thickness histogram argues against an impact origin (e.g., Andrews-Hanna et al., 2008), unless perhaps the basin has reached an advanced stage of horizontal relaxation.

There exist several alternative and more likely explanations for the lunar asymmetry, including thickening of the farside crust by ejecta from the South Pole–Aitken Basin (Zuber et al., 1994), degree-one mantle processes (Zhong et al., 2000), or a degree-one Rayleigh-Taylor instability developing in an over-dense ilmenite-rich cumulate layer in the upper mantle (Parmentier et al., 2002).

At this point, there is no compelling evidence in favor of either a Procellarum or nearside-encompassing basin on the Moon. However, the extensive geophysical data analysis required to isolate the Borealis Basin on Mars dictates that such large structures that date from earliest planetary evolution can be difficult to identify. That said, the existence of Borealis demonstrates the possibility of hemisphere-scale megabasins. The excellent preservation of the Borealis rim suggests a relatively late-stage impact (Andrews-Hanna and Zuber, 2008). Earlier mega impacts on all of the terrestrial planets during the late stages of accretion were likely, though such basins may be poorly preserved, if preserved at all, and difficult to recognize. While future work may confirm or deny the possible existence of these and other megabasins, we do not include them in this study.

Statistical Implications

The assumption that small crater statistics apply to these basins, with a 0.05 probability of a particular crater or basin having an elliptical shape, leads to a likelihood of only 8.5×10^{-5} that four of the six confirmed giant impact basins would be elliptical by random chance. Expansion of our definition of a giant impact basin to include all 11 well-characterized basins greater than 500 km diameter (six of which are elliptical) decreases the probability of finding six elliptical basins to 5.6×10^{-6}.

Clearly, the probability of elliptical crater formation observed for small craters cannot hold for the largest basins. If we assume that the probability of elliptical crater formation is independent of crater diameter (which we will later show to be false), we can calculate the probability of elliptical crater formation and the critical angle from the observed basins. The four out of six elliptical giant basins leads to a probability of elliptical basin formation of 0.67, corresponding to a critical angle of 54°. For the 11 well-characterized impact basins greater than 500 km in diameter, the six elliptical basins suggest that the probability that a given basin will be elliptical is ~0.55, corresponding to a critical angle of 48°. In the next section, we develop a simple geometrical model for the critical angle of elliptical crater and basin formation, which will then be compared to the observed population of elliptical craters and basins.

MODEL

The basis of our conceptual model is similar to that of Bottke et al. (2000). Oblique impacts onto the surface of a planet result in an elongated projectile footprint, with an aspect ratio of $a/b = 1/\sin(\theta)$ for the case of a projectile that is small relative to the size of the planet. The excavation cavity then expands outwards from this projectile footprint, and the final postmodification crater aspect ratio (A/B) will be a function of both the aspect ratio of the projectile footprint and the ratio between the final crater diameter and the projectile diameter (D_c/d_p). However, while Bottke et al. (2000) used this conceptual model to constrain a semi-empirical power-law relationship between θ_c and D_c/d_p based on experimental results, we use this geometric approach to estimate the crater aspect ratio as a function of impact angle and size for both the experimental results and the observed crater and basin populations on the terrestrial planets. This model also takes into account the effect of the curvature of the planet's surface on the resulting crater shape, allowing its application to the formation of giant impact basins.

For the case of a curved planetary surface, the projectile footprint aspect ratio depends on both the impact angle and the sizes of the projectile and target planet. We calculate this aspect ratio geometrically, as a function of the impact angle at the point of first contact between the projectile and target (defining the impact angle as such preserves the $\sin^2\theta$ dependence of the probability). It can be shown that the x-coordinate of the point of intersection of the top/bottom of the projectile (defined as the two points on the projectile surface tangential with the direction of motion and aligned in the same vertical plane as the point of first impact) with the surface of the planet is given by:

$$x_{\pm} = \frac{-b + \sqrt{b^2 - 4ac}}{2a},$$

where

$$a = \tan^2\theta + 1,$$

$$b = \mp 2r\sin\theta\tan^2\theta - 2\tan\theta(R + r \pm r\cos\theta), \text{ and}$$

$$c = r^2\sin^2\theta\tan^2\theta \pm 2r\sin\theta\tan\theta(R + r \pm r\cos\theta)$$

$$(R + r \pm r\cos\theta)^2 - R^2, \quad (2)$$

and where r is the radius of the projectile, R is the planetary radius, and the top sign in each sign pair applies to the projectile top. From this, the projectile footprint dimensions can be calculated as:

$$a = R\cdot\left[\arcsin\left(\frac{x_+}{R}\right) + \arcsin\left(\frac{x_-}{R}\right)\right]$$

$$b = 2R\cdot\arcsin\left(\frac{r}{R}\right). \quad (3)$$

For the special case of $R = \infty$, the aspect ratio from Equations 2 and 3 reduces to $1/\sin(\theta)$, as predicted for a flat planet.

The projection of a spherical projectile onto the surface of a planet results in a highly centralized mass/energy distribution within the projectile footprint, with the projectile mass decreasing to zero at the edges (Fig. 2). We scale the projectile footprint down by a factor γ to account for this nonuniform mass distribution:

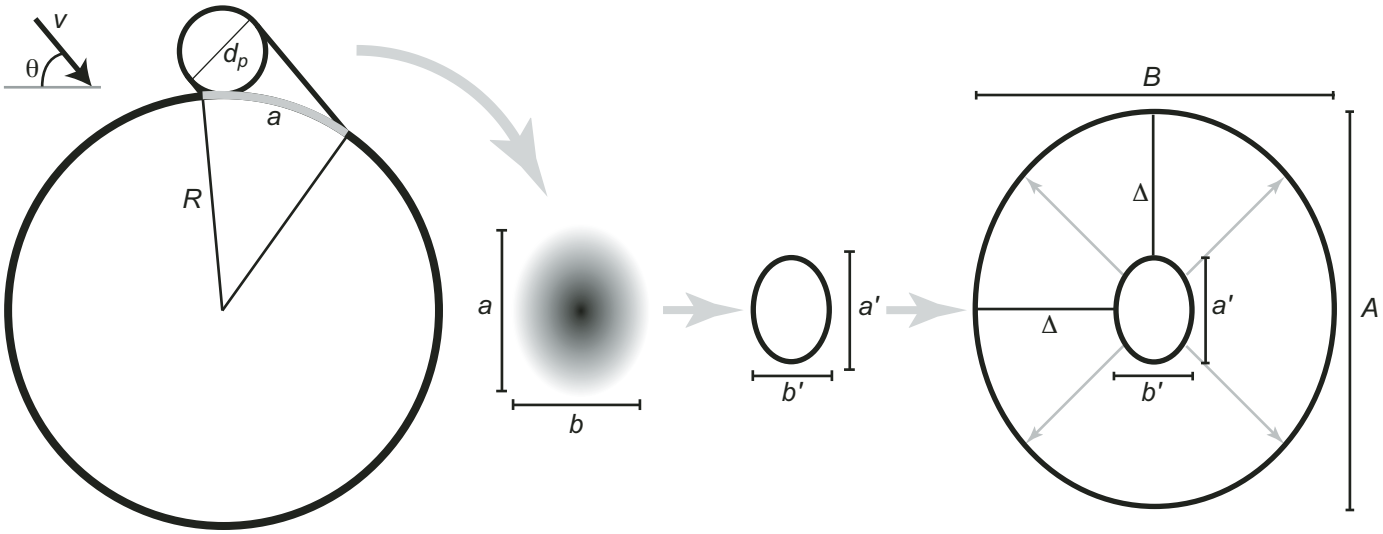

Figure 2. Diagram of the conceptual model, in which a projectile of diameter d_p strikes a planet of radius R at velocity v and impact angle θ, producing a projectile footprint of aspect ratio a/b characterized by a centrally condensed mass distribution. The basin cavity is assumed to expand outward from the scaled projectile footprint, a'/b', by a uniform amount Δ in the radial direction to create a crater of aspect ratio A/B.

$$\left(a',b'\right)=\gamma\cdot\left(a,b\right)$$

$$\gamma=\frac{\int_0^R \rho(r)\,r\,dr}{R\cdot\int_0^R \rho(r)\,dr}=\frac{\int_0^R \left(R^2-r^2\right)^{1/2} r\,dr}{R\cdot\int_0^R \left(R^2-r^2\right)^{1/2} dr}=\frac{4}{3\pi}, \quad (4)$$

where ρ(*r*) is the surface mass density within a circular projectile footprint as a function of the radial distance *r* from the center of the footprint. While this scaling is an ad hoc correction, some justification is garnered from the success of the model in reproducing both the experimental results and the observed fraction of elliptical craters, as will be seen in the next section. This scaling factor is formulated such that if all of the mass of the projectile were concentrated as a delta function at $r = R$, γ would equal 1. Using a total mass weighting rather than density weighting (replacing ρ[*r*] with $2\pi r\rho[r]$ in Eq. 4), overestimates the final crater ellipticity for the small crater population. Alternatively, we can numerically integrate the energy radiating outwards from each point in the footprint and assume that the final crater rim is an iso-energy surface, though this underestimates the final crater aspect ratio.

We assume that the scaled projectile footprint expands uniformly in all directions by a distance Δ in order to reach the mean crater diameter predicted by the scaling relationships (Fig. 2). Most studies adopt the π-scaling relationships, in which the final mean crater diameter (D_c) is calculated as (Melosh, 1989; Bottke et al., 2000):

$$D_c=1.25\cdot C_D d_p^{\,1-\beta}\left(\frac{\frac{1}{6}\pi\rho_p}{\rho_t}\sin\theta\right)^{1/3}\left(\frac{1.61g}{V^2}\right)^{-\beta}, \quad (5)$$

where C_D is a drag coefficient, ρ_p is the projectile density, ρ_t is the target density, θ is the impact angle measured from horizontal, g is the gravitational acceleration of the target planet, V is the impact velocity, and β is a constant. The factor of 1.25 accounts for the enlargement of complex craters relative to the transient cavity (Melosh, 1989), though the applicability of this scaling to basins is uncertain. The sin θ dependence has been added to account for the effect of impact angle on mean crater diameter (Gault and Wedekind, 1978).

Alternative scaling relationships are often used. In a study of the formation of the Borealis Basin on Mars, Marinova et al. (2008) found that the results of their smooth particle hydrodynamics (SPH) models agreed better with the energy scaling relationship used by Wilhelms and Squyres (1984):

$$D_c=K\cdot\left(E\cdot\sin\theta\right)^{\alpha} g^{-1/6}, \quad (6)$$

where E is the impact energy, K equals 0.0348 (mks units), α equals 0.29 (Housen et al., 1979), and we have introduced the sin θ dependence into the energy term (Gault and Wedekind, 1978). This scaling relationship diverges from the π-scaling relationship for large basins, resulting in a difference in predicted projectile diameter for a given crater of up to a factor of 3 for the largest hemisphere-scale basins. While the π-scaling relationship is preferred for small craters, it may greatly underestimate the expansion of the basin from the projectile footprint for the largest impacts. The uncertainty in the relationship between projectile

diameter/energy and basin size also extends to numerical simulations. Nimmo et al. (2008) found that the projectile diameter required to produce a Borealis-sized basin in SPH simulations was twice that required by their finite-element model. There is clearly still much that remains to be learned regarding the dynamics of giant basin excavation.

We here consider both the π-scaling relationship and the energy scaling relationship, though we will focus primarily on the former in the discussion that follows. While the uncertain applicability of these scaling relationships to basin-forming impacts introduces significant uncertainty in the specific numerical results of this study, this approach allows us to characterize the effect of planetary curvature on basin shape and to efficiently investigate a wide range of parameter space. The general conclusions of this work are not sensitive to this uncertainty.

Given the projectile footprint dimensions and the predicted final mean basin diameter based on the scaling relationships, we can calculate the aspect ratio of the crater ε_{crater} as:

$$\varepsilon_{crater} = \frac{a' + \Delta}{b' + \Delta}$$
$$\Delta = D_c - \frac{a' + b'}{2} \quad . \qquad (7)$$

Note that both the aspect ratio of the impact footprint and the mean final crater diameter depend on the impact angle. Previous inventories of craters have generally assumed a threshold aspect ratio of 1.2 for classification as an elliptical crater (e.g., Bottke et al., 2000), and we adopt this value here as well.

While this first-order geometrical model is greatly oversimplified, it will be shown in the next section that it successfully predicts the onset of crater ellipticity both in laboratory experiments and in the observed population of small craters on the terrestrial planets, thus justifying its application to the larger impact basins.

RESULTS

Experimentally Produced Elliptical Craters

We first apply this model to the experimental study of oblique impact cratering of Gault and Wedekind (1978). That study fired 1.6–12.5-mm-diameter aluminum and Pyrex spheres at a target of unconsolidated quartz sand at velocities ranging from 3.6 to 7.2 km/s. In our analysis, we assume the mean impact velocity of 5.4 km/s for 1 and 10 mm spheres, with projectile (2700 kg/m^3) and target (1700 kg/m^3) densities appropriate for aluminum and quartz sand, and values of β (0.17) and C_D (1.68) appropriate for quartz sand (Melosh, 1989) (Table 2). We find that our simple geometrical model accurately predicts the crater aspect ratio over the full range of impact angles (Fig. 3).

TABLE 2. SUMMARY OF PARAMETERS USED IN MODELS

	Experimental	Planetary
Target material	Quartz sand	Rock/wet sand
Drag coefficient (C_D)*	1.4	1.6
b*	0.16	0.22
Target density (ρ_t)	1700 kg/m^3	2700 kg/m^3
Projectile material	Aluminum/Pyrex	Chondrite
Projectile density (ρ_p)	2700 kg/m^3	2200 kg/m^3
Impact velocity (V)	5.4 km/s	12 km/s

*Constants governing the π-scaling relationship in Equation 5.

Elliptical Crater and Basin Predictions for Mars

In this and the following sections, we will discuss the results from the π-scaling calculations, though results from the alternative energy scaling are also presented in Table 1. For all planetary crater scaling calculations, we assume values of β (0.22) and C_D (1.6) appropriate for wet sand or rock, as in Melosh (1989) and Bottke et al. (2000). Choosing instead target parameters determined from impacts into dry quartz sand, which may be more appropriate for gravity-regime craters, does not significantly change the results. We assume projectile (2200 kg/m^3) and target (2700 kg/m^3) densities appropriate for chondritic and crustal materials, respectively. Projectile velocities are assumed to be 12 km/s, comparable to estimated velocities of asteroids striking the Moon and Mars (Bottke et al., 1994, 2000).

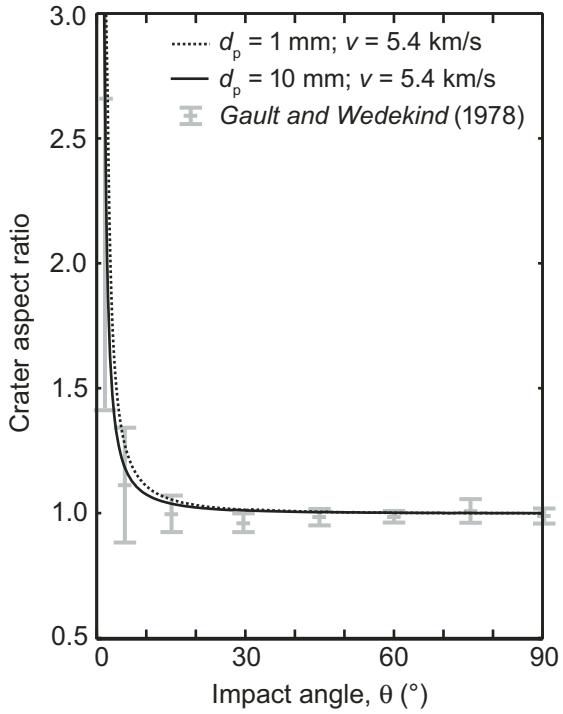

Figure 3. Comparison of predicted crater aspect ratio to the experimental results of Gault and Wedekind (1978). Gault and Wedekind (1978) used aluminum and Pyrex spheres with diameters between 1.6 and 12.5 mm, fired into quartz sand at 3.6–7.2 km/s. Calculations used π-scaling relationships assuming projectile diameters of 1 and 10 mm, fired into quartz sand at 5.4 km/s.

In order to highlight the effect of the curvature of the planetary surface, we first consider the case of a "flat Mars," in which the curvature of the planet is neglected. The projectile footprint aspect ratio is independent of projectile size and follows the simple 1/sin θ dependence (Fig. 4A). For this case, the critical angle for elliptical crater formation still increases with increasing crater size, as pointed out by Bottke et al. (2000). Larger projectiles result in a lower D_c/d_p ratio, decreasing the enlargement of the crater beyond the impact footprint (Δ) relative to the projectile diameter (d_p). For small impactors (d_p ~1 km; D_c ~10 km), the critical angle for elliptical crater formation is predicted to be 13°, corresponding to a probability of $\theta < \theta_c$ of $P = 0.05$ (Fig. 4C), which is in agreement with the observed 5% abundance on the terrestrial planets. As the projectile and crater sizes increase, however, the critical angle for elliptical crater formation increases to 30° for a 1000-km-diameter projectile (producing a basin roughly 50% larger than Hellas or Utopia), corresponding to a 0.25 probability of ellipticity.

Upon including the effect of the curvature of the planet's surface, the projectile footprint aspect ratio becomes dependent upon both the impact angle and the projectile and planet diameters (Fig. 4D). For Mars, this effect begins to be significant for projectile diameters greater than ~100 km. A projectile diameter of 1000 km now leads to a critical angle of 43°, with a corresponding probability of 0.47. For large impactors on highly oblique trajectories, the curvature of the planet also increases the likelihood of a glancing or decapitating impact, in which a portion of the projectile misses the surface altogether (Schultz and

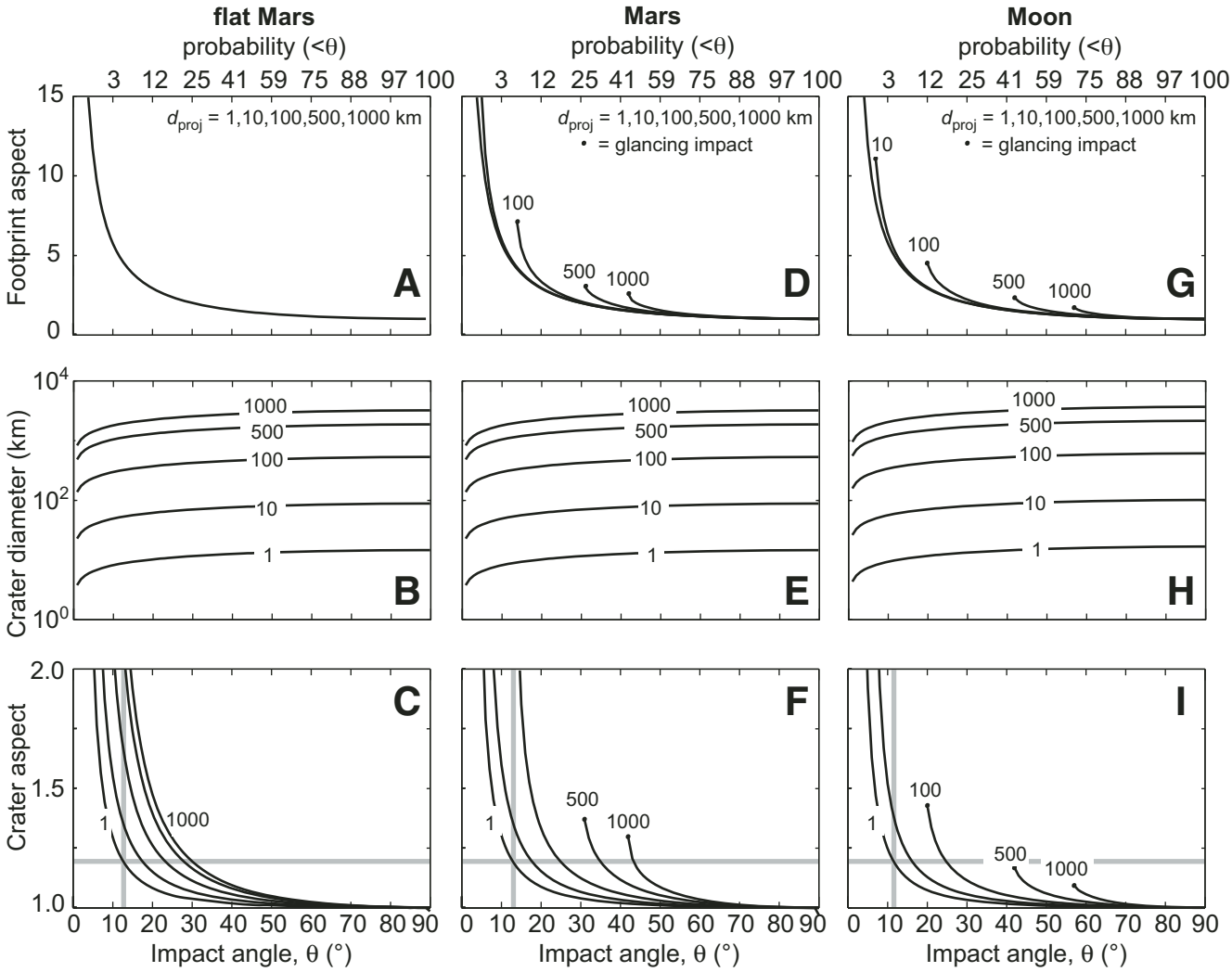

Figure 4. Predicted projectile footprint aspect ratio, crater diameter, and crater aspect ratio for craters on Mars neglecting surface curvature (A–C), Mars including effects of surface curvature (D–F), and the Moon including effects of surface curvature (G–I). The final crater diameters here are based on the π-scaling relationship. Projectiles range in diameter from 1 to 1000 km. Projectile and target properties are as given in Table 2. The vertical and horizontal gray lines in the bottom panels indicate the critical angle corresponding to the observed 5% abundance of elliptical craters on the terrestrial planets, and the assumed threshold aspect ratio of 1.2 for consideration as elliptical, respectively.

Crawford, 2008). The critical angle for a decapitating impact of a 1000-km-diameter projectile on Mars is 42° (P = 0.45). These decapitating impacts would likely affect the resulting crater morphology and encourage elliptical crater formation. While both scaling analyses and the geometric method in this study are inapplicable to decapitating impacts, the formation of an elliptical basin would be a likely outcome, since the projectile would be traveling parallel to the surface at the down-range edge of the projectile footprint, leading to a pronounced down-range focusing of the impact energy and basin excavation.

We now consider the observed population of giant impact basins on Mars (Table 1). The critical angle for producing an elliptical basin for the Isidis impact (D_c = 1500 km) is θ_c = 34°, with a probability of $\theta < \theta_c$ of 0.31. For Argyre (D_c = 780 km), the critical angle and probability are reduced to 29° and 0.24, respectively. The larger Hellas and Utopia (D_c = 1940–2220 km) impacts would have had a critical angle of 38°–40°, occurring with a probability of 0.38–0.41. However, the critical angle for projectile decapitation would have been 35°–37°, with a probability of 0.34–0.36. Given that these basins are known to be elliptical, projectile decapitation was likely. For the Borealis Basin, the critical angle for projectile decapitation of 78° (P = 0.96) occurs before the onset of elliptical crater formation. If the energy scaling relationship is adopted, the probabilities of elliptical basin formation for Hellas, Utopia, and Borealis are decreased to 0.15, 0.17, and 0.62, respectively.

Elliptical Crater and Basin Predictions for the Moon and Mercury

The smaller size of the Moon results in an increased likelihood that a basin of a given diameter will be elliptical upon taking into consideration the curvature of the surface. The critical angle for a 100-km-diameter projectile is 24.5° (P = 0.17). For the South Pole–Aitken Basin, the critical angle for elliptical crater formation is roughly the same as that for projectile decapitation of 44° (P = 0.48), suggesting that projectile decapitation would have likely occurred in the South Pole–Aitken–forming impact. The smaller Crisium, Serenitatis, Nubium, and Imbrium Basins have θ_c = 25°–33° (P = 0.18–0.30). Applying the model to Mercury, we find that θ_c for the Caloris-forming impact would have been 33° (P = 0.30).

Statistical Comparison with Observed Population of Elliptical Basins

The probabilities of elliptical crater formation for the individual basins in Table 1 can be used to calculate the most probable number of elliptical basins given the size distribution in the population of giant basins using a simple Monte Carlo approach. In this analysis, we are not concerned with which particular basins are elliptical, though the larger basins are significantly more likely to be elongated. For the six largest confirmed impact basins (Borealis, Hellas, Utopia, South Pole–Aitken, Imbrium, and Caloris), the probabilities in Table 1 suggest that 2.8 ± 1.1 (1σ uncertainty) of these basins would be expected to be elliptical, which is less than the observed four elliptical basins but within the 2σ uncertainty. If we expand the definition of a giant impact basin to include all 11 well-characterized basins greater than 500 km in diameter on the Moon, Mercury, and Mars (Borealis, Hellas, Utopia, Isidis, Argyre, South Pole–Aitken, Imbrium, Serenitatis, Nubium, Crisium, and Caloris), the expected outcome is 4.0 ± 1.4 elliptical basins, which is again less than the observed six elliptical basins, but within the 2σ uncertainty. Given the small sample sizes, these results are generally consistent with the observed population of elliptical basins, though they suggest that this work may underestimate the probability of elliptical basin formation for the largest impacts.

The effect of the curvature of the planet's surface is most evident when comparing the probability of elliptical crater formation as a function of the crater diameter for the equivalent vertical impact (Fig. 5). The results for a flat Mars compare well with those of Bottke et al. (2000), and the critical angle for elliptical crater formation follows a power law of the form in Equation 1, with θ_0 equal to 54.6° and m equal to –0.543, similar to the values derived in that study (Fig. 5A). For the case of a flat planet, the probability of elliptical crater formation increases only modestly for basin diameters greater than ~1000 km (Fig. 5B) as a result of the power-law form of the relationship. In contrast, for the curved

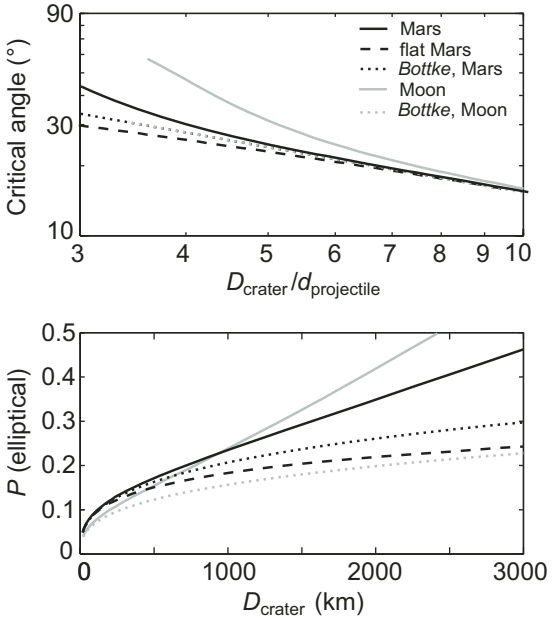

Figure 5. Relationship between θ_c and D_c/d_p (based on the π-scaling relationship), and between the probability of elliptical crater formation and the crater diameter for Mars, Mars with neglecting effects of planetary curvature ("flat Mars"), and the Moon. Power-law relationships from Bottke et al. (2000) for the Moon and Mars are shown for comparison (the Mars and Moon curves are coincident in the top panel).

surfaces of Mars and the Moon, the probability continues to rise steadily with increasing basin diameters, leading to a significant departure from the power law of Equation 1. On the Moon, the probability of a South Pole–Aitken–sized basin being elliptical is more than twice what it would be if the curvature of the surface were neglected (P = 0.43 and 0.18, respectively), while the probability of a Hellas-sized basin on Mars being elliptical is nearly doubled when the curvature of the planet is included (P = 0.40 versus 0.24).

DISCUSSION

This work has shown that there is a clear tendency for the largest impact basins in the solar system to have an elliptical rather than circular shape. The Borealis, Hellas, Utopia, and South Pole–Aitken Basins on Mars and the Moon have aspect ratios ranging from 1.2 to 1.4. Of the basins we classify as giant impact basins, only Caloris and Imbrium fall short of the assumed threshold aspect ratio of 1.2 for classification as elliptical, though even these basins display clear departures from circularity.

We explain this predominance of elliptical giant impact basins as resulting from the effects of the curvature of the planets' surfaces. The simple geometric approach taken here, which builds on the work of Bottke et al. (2000), can to first order explain the results of both small-scale cratering experiments and the observed population of small elliptical craters on the terrestrial planets. Application of this approach to the giant basin–forming impacts demonstrates that curvature of the planetary surfaces leads to a significant increase in the likelihood of formation of basins with an elliptical shape by increasing the aspect ratio of the projectile footprint, thereby increasing the effective obliqueness of the entry angle of the impact. This work predicts that the probability that any one of the three largest confirmed impact basins (Hellas, Utopia, and South Pole–Aitken) would be elliptical is ~0.4, while the much larger Borealis Basin on Mars would have had a probability of being elliptical approaching unity.

In the population of 11 well-characterized impact basins greater than 500 km in diameter considered here, this analysis suggests that between two and six elliptical basins would be expected, consistent with the observed six elliptical basins. If one considers only the six largest giant impact basins, this analysis would predict that between two and four basins should be elliptical, again consistent with the observed four elliptical basins, though this calculation is clearly compromised by the statistics of small numbers. While generally consistent with the occurrence of elliptical giant impact basins, these results suggest that this work may underestimate the predicted ellipticity of the largest basins. A possible explanation may lie in the simplistic assumption that the crater is excavated uniformly in all directions from the projectile footprint. In oblique impacts, there is a pronounced downrange focusing of the impact energy, with the isobaric core elongating and remaining close to the surface (Pierazzo and Melosh, 2000a). For very large and oblique impacts, this isobaric core would likely re-intersect the planetary surface. The excavation process in these cases would be strongly focused down range, likely favoring crater elongation and decreasing the critical angle for elliptical basin formation (Garrick-Bethell and Zuber, 2009). Alternatively, it is possible that at the scale of the largest basins, the larger melt volume produced by less oblique impacts may prevent basin preservation (Marinova et al., 2008), thus biasing the population of preserved basins toward higher aspect ratios.

Another factor that can contribute to crater elongation is the projectile density, through its effect on the ratio between the crater and projectile diameters. It has been suggested that the late heavy bombardment may have resulted from an influx of both asteroids and icy bodies from the outer solar system that were destabilized by the outward migration of the giant planets (Gomes et al., 2005; Strom et al., 2005). Low-density icy projectiles would lead to a lower D_c/d_p ratio, increasing the probability of elliptical basin formation, though the higher impact velocities would counter this effect. Alternately, the largest projectiles would be expected to be more compacted and thus denser than the assumed uncompressed chondritic density, thereby decreasing the resulting crater ellipticity. However, basin-forming impacts may also excavate into the dense mantle, tending to decrease the size and increase the ellipticity of the resulting basin. Impact velocity also plays a key role, with slower projectiles predicting more elliptical craters due to both the decreased D_c/d_p ratio and the greater influence of the planetary curvature for the larger projectiles required to produce a basin of a given diameter.

Despite the success of this simple approach in explaining the elliptical crater population observed both experimentally and on the surfaces of the planets, it cannot capture the full complexity of the impact and excavation process. This work suffers the limitation that it relies on extrapolating scaling relationships by many orders of magnitude to apply them to basin-forming impacts. The validity of this extrapolation is questionable, even for the limit of a flat planet, and the curvature of the surface would likely further affect the relationship between mean crater diameter and impact energy. Nevertheless, this work underscores the importance of both the size of the impact and the curvature of the surface in determining the resulting morphology of giant impact basins. Much work remains to be done to understand the process of giant impact basin formation and modification.

This work has focused on the basin shape, demonstrating that the curvature of the planetary surfaces increases the likelihood of elliptical crater formation at the scale of giant impact basins, essentially increasing the effective obliqueness of the impact. Many aspects of crater morphology are dependent upon the angle of impact, including crater ellipticity, ejecta distribution, and the amount of impact melt (Pierazzo and Melosh, 2000b). Small-scale laboratory experiments and numerical simulations of impacts into generally flat targets reveal a progression of crater and ejecta morphology with decreasing impact angle. Impacts at angles less than ~30° produce asymmetric ejecta; impacts at angles less than 15°–30° produce dramatically less impact melt relative to the crater volume; impacts at angles less than 10°–15° produce elliptical craters; and impacts at angles

less than 5°–10° produce "butterfly" ejecta blankets displaced down range with large forbidden zones (Pierazzo and Melosh, 2000b). This work on crater elongation suggests that at least one step in this progression is not universal, but rather depends on both the ratio of the crater to projectile size and the radius of curvature of the planet. For the case of the large basin-forming impacts, a large fraction (and possibly the majority) of impacts must be considered to be "highly oblique" on account of the curvature of the planetary surface.

ACKNOWLEDGMENTS

This paper benefited from thorough and thoughtful reviews by Herbert Frey and Bradley Thomson. This work was supported by a National Aeronautics and Space Administration (NASA) Planetary Geology and Geophysics Grant to Zuber.

REFERENCES CITED

Andrews-Hanna, J.C., and Zuber, M.T., 2008, The dichotomy-forming impact on Mars: Evidence and implications, *in* Workshop on the Early Solar System Impact Bombardment: LPI Contribution No. 1439, Houston, Texas, p. 13–14.

Andrews-Hanna, J.C., Zuber, M.T., and Banerdt, W.B., 2008, The Borealis Basin and the origin of the Martian crustal dichotomy: Nature, v. 453, p. 1212–1215, doi: 10.1038/nature07011.

Archinal, B.A., Rosiek, M.R., Kirk, R.L., and Redding, B.L., 2006, The Unified Lunar Control Network 2005: U.S. Geological Survey Open-File Report 2006–1367, 18 p.

Banerdt, W.B., 1986, Support of long-wavelength loads on Venus and implications for internal structure: Journal of Geophysical Research, v. 91, p. 403–419, doi: 10.1029/JB091iB01p00403.

Banerdt, W.B., and Golombek, M.P., 2000, Tectonics of the Tharsis region of Mars: Insights from MGS topography and gravity: Lunar and Planetary Science Conference Proceedings, v. 31, abstract 2038.

Barlow, N.G., 1988, Crater size-frequency distributions and a revised Martian relative chronology: Icarus, v. 75, p. 285–305, doi: 10.1016/0019-1035(88)90006-1.

Bottke, W.F., Nolan, M.C., Greenburg, R., and Kolvoord, R.A., 1994, Collisional lifetimes and impact statistics of near-Earth asteroids, *in* Gehrels, T., Matthews, M.S., and Schumann, A.M., ed., Hazards Due to Comets and Asteroids: Tucson, University of Arizona Press, p. 337–357.

Bottke, W.F., Love, S.G., Tytell, D., and Glotch, T., 2000, Interpreting the elliptical crater populations on Mars, Venus, and the Moon: Icarus, v. 145, p. 108–121, doi: 10.1006/icar.1999.6323.

Byrne, C.J., 2007, A large basin on the near side of the Moon: Earth, Moon, and Planets, v. 101, p. 153–188, doi: 10.1007/s11038-007-9225-8.

Cadogan, P.H., 1974, Oldest and largest lunar basin?: Nature, v. 250, p. 315–316, doi: 10.1038/250315a0.

Christiansen, E.L., Cytowski, E.D., and Ortega, J., 1993, Highly oblique impacts into thick and thin targets: International Journal of Impact Engineering, v. 14, p. 157–168, doi: 10.1016/0734-743X(93)90017-2.

Fassett, C.I., Head, J.W., Blewett, D.T., Chapman, C.R., Dickson, J.L., Murchie, S.L., Solomon, S.C., and Watters, T.R., 2009, Caloris impact basin: Exterior geomorphology, stratigraphy, morphometry, radial sculpture, and smooth plains deposits: Earth and Planetary Science Letters, v. 285, p. 297–309.

Frey, H.V., 2006, Impact constraints on, and a chronology for, major events in early Mars history: Journal of Geophysical Research, v. 111, p. E08S91, doi: 10.1029/2005JE002449.

Frey, H.V., 2008a, Ages of very large impact basins on Mars: Implications for the late heavy bombardment in the inner solar system: Geophysical Research Letters, v. 35, p. L13203, doi: 10.1029/2008GL033515.

Frey, H.V., 2008b, Previously unrecognized lunar impact basins revealed by topographic data: Lunar and Planetary Science Conference Proceedings, v. 39, abstract 1344.

Frey, H.V., Roark, J.H., Shockey, K.M., Frey, E.L., and Sakimoto, S.E.H., 2002, Ancient lowlands on Mars: Geophysical Research Letters, v. 29, no. 10, doi: 10.1029/2001GL013832.

Garrick-Bethell, I., and Zuber, M.T., 2009, Elliptical structure of the lunar South Pole-Aitken basin: Icarus, v. 204, p. 399–408.

Gault, D.E., and Wedekind, J.A., 1978, Experimental studies of oblique impacts: Lunar and Planetary Science Conference Proceedings, v. 5, p. 3843–3875.

Gilbert, G.K., 1893, The moon's face, a study of the origin of its features: Bulletin of the Philosophical Society of Washington, v. 12, p. 241–292.

Gomes, R., Levison, H.F., Tsiganis, K., and Morbidelli, A., 2005, Origin of the cataclysmic late heavy bombardment period of the terrestrial planets: Nature, v. 435, p. 466–469, doi: 10.1038/nature03676.

Hikida, H., and Wieczorek, M.A., 2007, Crustal thickness of the Moon: New constraints from gravity inversions using polyhedral shape models: Icarus, v. 192, p. 150–166, doi: 10.1016/j.icarus.2007.06.015.

Holsapple, K.A., and Schmidt, R.M., 1982, On the scaling of crater dimensions: 2. Impact processes: Journal of Geophysical Research, v. 87, p. 1849–1870, doi: 10.1029/JB087iB03p01849.

Housen, K.R., Wilkening, L.L., Chapman, C.R., and Greenberg, R., 1979, Asteroidal regoliths: Icarus, v. 39, p. 317–351, doi: 10.1016/0019-1035(79)90145-3.

Lawrence, D.J., Feldman, W.C., Elphic, R.C., Little, R.C., Prettyman, T.H., Maurice, S., Lucey, P.G., and Binder, A.B., 2002, Iron abundances on the lunar surface as measured by the *Lunar Prospector* gamma-ray and neutron spectrometers: Journal of Geophysical Research, v. 107, p. 5130, doi: 10.1029/2001JE001530.

Lawrence, D.J., Elphic, R.C., Feldman, W.C., and Prettyman, T.H., 2003, Small-area thorium features on the lunar surface: Journal of Geophysical Research, v. 108, p. 5102, doi: 10.1029/2003JE002050.

Marinova, M.M., Aharonson, O., and Asphaug, E., 2008, Mega-impact formation of the Mars hemispheric dichotomy: Nature, v. 453, p. 1216–1219, doi: 10.1038/nature07070.

McGill, G.E., 1989, Buried topography of Utopia, Mars: Persistence of a giant impact depression: Journal of Geophysical Research, v. 94, p. 2753–2759, doi: 10.1029/JB094iB03p02753.

McGill, G.E., and Squyres, S.W., 1991, Origin of the Martian crustal dichotomy: Evaluating hypotheses: Icarus, v. 93, p. 386–393, doi: 10.1016/0019-1035(91)90221-E.

Melosh, H.J., 1989, Impact Cratering: A Geologic Process: Oxford Monographs on Geology and Geophysics, v. 11, 245 p.

Mohit, P.S., and Phillips, R.J., 2007, Viscous relaxation on early Mars: A study of ancient impact basins: Geophysical Research Letters, v. 34, p. L21204, doi: 10.1029/2007GL031252.

Murchie, S.L., Watters, T.R., Robinson, M.S., Head, J.W., Strom, R.G., Chapman, C.R., Solomon, S.C., McClintock, W.E., Proktor, L.M., Domingue, D.L., and Blewett, D.T., 2008, Geology of the Caloris Basin, Mercury: A view from *Messenger*: Science, v. 321, p. 73–76, doi: 10.1126/science.1159261.

Neumann, G.A., Lemoine, F.G., Smith, D.E., and Zuber, M.T., 2008, Marscrust3—A crustal thickness inversion from recent MRO gravity solutions: Lunar and Planetary Science Conference Proceedings, v. 39, abstract 1391.

Nimmo, F., Hart, S.D., Korycansky, D.G., and Agnor, C.B., 2008, Implications of an impact origin for the Martian hemispheric dichotomy: Nature, v. 453, p. 1220–1223, doi: 10.1038/nature07025.

Parmentier, E.M., Zhong, S., and Zuber, M.T., 2002, Gravitational differentiation due to initial chemical stratification: Origin of lunar asymmetry by the creep of dense KREEP?: Earth and Planetary Science Letters, v. 201, p. 473–480, doi: 10.1016/S0012-821X(02)00726-4.

Phillips, R.J., Arvidson, R.E., Boyce, J.M., Campbell, D.B., Guest, J.E., Schaber, G.G., and Soderblom, L.A., 1991, Impact craters on Venus: Initial analysis from *Magellan*: Science, v. 252, p. 288–297, doi: 10.1126/science.252.5003.288.

Pierazzo, E., and Melosh, H.J., 2000a, Melt production in oblique impacts: Icarus, v. 145, p. 252–261, doi: 10.1006/icar.1999.6332.

Pierazzo, E., and Melosh, H.J., 2000b, Understanding oblique impacts from experiments, observations, and modeling: Annual Review of Earth and Planetary Sciences, v. 28, p. 141–167, doi: 10.1146/annurev.earth.28.1.141.

Schultz, P.H., and Crawford, D.A., 2008, Impactor survivors as additional sources for the late heavy bombardment, *in* Workshop on the Early Solar System Impact Bombardment: LIP Contribution No. 1439, Houston, Texas, p. 55–56.

Schultz, P.H., and Lutz-Garihan, A.B., 1982, Grazing impacts on Mars: A record of lost satellites: Journal of Geophysical Research, v. 87, p. A84–A96, doi: 10.1029/JB087iS01p00A84.

Searls, M.L., Banerdt, W.B., and Phillips, R.J., 2006, Utopia and Hellas Basins, Mars: Twins separated at birth: Journal of Geophysical Research, v. 111, no. E8, p. E08005, doi: 10.1029/2005JE002666.

Shoemaker, E.M., 1962, Interpretation of lunar craters, *in* Kopal, Z., ed., Impact and Explosion Cratering: New York, Pergamon, p. 1–10.

Smith, D.E., Zuber, M.T., Neumann, G.A., and Lemoine, F.G., 1997, Topography of the Moon from *Clementine* lidar: Journal of Geophysical Research, v. 102, p. 1591–1612, doi: 10.1029/96JE02940.

Smith, D.E., Sjorgren, W.L., Tyler, G.L., Balmino, G., and Lemoine, F.G., 1999, The gravity field of Mars: Results from the *Mars Global Surveyor*: Science, v. 286, p. 94–96, doi: 10.1126/science.286.5437.94.

Smith, D.E., Zuber, M.T., Frey, H.V., Garvin, J.B., Head, J.W., Muhleman, D.O., Pettengill, G.H., Phillips, R.J., Solomon, S.C., Zwally, H.J., Banerdt, W.B., Duxbury, T.C., Golombek, M.P., Lemoine, F.G., Neumann, G.A., Rowlands, D.D., Aharonson, O., Ford, P.G., Ivanov, A.B., McGovern, P.J., Abshire, J.B., Afzal, R.S., and Sun, X., 2001, Orbiter Laser Altimeter (MOLA): Experiment summary after the first year of global mapping of Mars: Journal of Geophysical Research, v. 106, p. 23,689–23,722, doi: 10.1029/2000JE001364.

Smith, D.E., Zuber, M.T., Jackson, G.B., Cavanaugh, J.F., Neumann, G.A., Riris, H., Sun, X., Zellar, R.S., Coltharp, C., Connely, J., Katz, R.B., Kleyner, I., Liiva, P., Matuszeski, A., Mazarico, E.M., McGarry, J.F., Novo-Gradac, A.-M., Ott, M.N., Peters, C., Romos-Izquierdo, LA., Ramsey, L., Rolands, D.D., Schmidt, S., Scott, V.S., Shaw, G.B., Smith, J.C., Swinski, J.-P., Torrence, M.H., Unger, G., Yu, A.W., and Zagwodzki, T.W., 2009a, The Lunar Orbiter Laser Altimeter Investigation on the Lunar Reconnaissance Orbiter Mission, Space Sci., Rev., doi: 10.1007/s11214-009-9512-y.

Smith, D.E., Zuber, M.T., Neumann, G.A., Mazarico, E., Torrence, M.H., Westbrook, O.W., Head, J.W., Aharonson, O., Robinson, M.S., Cavanaugh, J.F., Sun, X., Lemoine, F.G., Barnouin-Jha, O.S., Duxbury, T.C., Oberst, J., and Lucey, P.G., 2009b, Early results from the Lunar Orbiter Laser Altimeter on LRO, Eos Trans. AGU, v. 90, no. 52, Fall Meet. Suppl., Abstract U21C-05.

Spudis, P.D., 1993, The Geology of Multi-Ring Impact Basins: Cambridge, UK, Cambridge University Press, 263 p.

Strom, R.G., Malhotra, R., Ito, T., Yoshida, F., and Kring, D.A., 2005, The origin of planetary impactors in the inner solar system: Science, v. 309, p. 1847–1850, doi: 10.1126/science.1113544.

Tanaka, K.L., and Leonard, G.J., 1995, Geology and landscape evolution of the Hellas region of Mars: Journal of Geophysical Research, v. 100, p. 5407–5432, doi: 10.1029/94JE02804.

Thomson, B.J., and Head, J.W., 2001, Utopia Basin, Mars: Characterization of topography and morphology and assessment of the origin and evolution of basin internal structure: Journal of Geophysical Research, v. 106, p. 23,209–23,230, doi: 10.1029/2000JE001355.

Whitaker, E.A., 1980, The Lunar Procellarum Basin, *in* Conference on Multi-Ring Basins: Formation and Evolution: LPI Contribution No. 414, Houston, Texas, p. 101.

Wieczorek, M.A., and Phillips, R.J., 1999, Lunar multi-ring basins and the cratering process: Icarus, v. 139, p. 246–259, doi: 10.1006/icar.1999.6102.

Wilhelms, D.E., 1987, The Geological History of the Moon: U.S. Geological Survey Professional Paper 1348, 302 p.

Wilhelms, D.E., and Squyres, S.W., 1984, The Martian hemispheric dichotomy may be due to a giant impact: Nature, v. 309, p. 138–140, doi: 10.1038/309138a0.

Zhong, S., Parmentier, E.M., and Zuber, M.T., 2000, A dynamic origin for the global asymmetry of the lunar mare basalts: Earth and Planetary Science Letters, v. 177, p. 131–140, doi: 10.1016/S0012-821X(00)00041-8.

Zuber, M., 2008, Mars reconnaissance orbiter derived gravity data: NASA Planetary Data System, MRO-M-RSS-5-SDP-V1.0.

Zuber, M.T., Smith, D.E., Lemoine, F.G., and Neumann, G.A., 1994, The shape and internal structure of the Moon from the *Clementine* mission: Science, v. 266, p. 1839–1843, doi: 10.1126/science.266.5192.1839.

Zuber, M.T., Smith, D.E., Neumann, G.A., Mazarico, E., Torrence, M.H., Head, J.W., Aharonson, O., Westbrook, O.W., Sori, M.M., Talpe, M.J., Garrick-Bethell, I., Barnouin-Jha, O.S., Duxbury, T.C., Lemoine, F.G., Oberst, J., and Lucey, P.G., 2009, Structure and morphology of the Moon's South-Pole-Aitken Basin from the Lunar Orbiter Laser Altimeter (LOLOA), Eos Trans. AGU, v. 90, no. 52, Fall Meet. Suppl., Abstract U21C-06.

Manuscript Accepted by the Society 29 September 2009

Printed in the USA